

Energy efficiency of a flat-plate solar collector using thermally treated graphene-based nanofluids: Experimental study

Omer A Alawi¹, Haslinda Mohamed Kamar¹,
Hussein A Mohammed², AR Mallah³, and Omar A Hussein^{4,5}

Abstract

A covalent functionalization approach was utilized for the preparation of highly dispersed pentaethylene glycol-thermally treated graphene-water as the absorbing material inside a flat-plate solar collector. Four mass fractions of nanofluids were prepared (0.025, 0.05, 0.075, and 0.1 wt% pentaethylene glycol-thermally treated graphene-water). Graphene nanoparticles were characterized by energy dispersive X-ray analysis with a scanning electron microscope. Measurements of the thermophysical properties were subsequently carried out for the nanosuspensions. The raw investigation data were collected from an indoor flat-plate solar collector test setup. The experimental procedure included different sets of variables such as input temperatures of 303, 313, and 323 K; fluid mass flow rate of 0.00833, 0.01667, and 0.025 kg s⁻¹; and heat flow density of 500, 750, and 1000 W m⁻². The thermophysical tests of pentaethylene glycol-thermally treated graphene-water nanofluids showed a proportional increase against weight concentrations, while the specific heat power was reduced. The tests showed an increment in energy efficiency by increasing the fluid mass flow rate and heat input. By comparison, the thermal efficiency decreased with the increasing temperature of the fluid supply. Relative to the base fluid, the energy efficiency of pentaethylene glycol-thermally treated graphene/water-based flat-plate solar collector increased to 10.6%, 11%, and 13.1% at the three fluid mass flow rates. In conclusion, an exponential form was used to derive the thermal effectiveness of flat-plate solar collector based on the experimental data.

Keywords

Energy efficiency, flat-plate solar collector, few-layer graphene, pentaethylene glycol, thermophysical properties

Date received: 22 May 2020; accepted: 27 August 2020

Topic: Nanoparticles and Colloids

Topic Editor: Raphael Schneider

Associate Editor: Raphael Schneider

¹ Department of Thermofluids, School of Mechanical Engineering, Universiti Teknologi Malaysia, Skudai, Johor Bahru, Malaysia

² School of Engineering, School of Molecular and Life Sciences, Edith Cowan University, Joondalup, WA, Australia

³ Department of Mechanical Engineering, University of Malaya, Kuala Lumpur, Malaysia

⁴ Department of Mechanical Engineering, Universiti Teknologi PETRONAS, Bandar Seri Iskandar, Perak Darul Ridzuan, Malaysia

⁵ Mechanical Engineering Department, College of Engineering, Tikrit University, Tikrit, Iraq

Corresponding authors:

Omer A Alawi and Haslinda Mohamed Kamar, Department of Thermofluids, School of Mechanical Engineering, Universiti Teknologi Malaysia, 81310 UTM Skudai, Johor Bahru, Malaysia.

Emails: omeralawi@utm.my; haslinda@utm.my; haslinda@mail.fkm.utm.my



Creative Commons CC BY: This article is distributed under the terms of the Creative Commons Attribution 4.0 License (<https://creativecommons.org/licenses/by/4.0/>) which permits any use, reproduction and distribution of the work without

further permission provided the original work is attributed as specified on the SAGE and Open Access pages (<https://us.sagepub.com/en-us/nam/open-access-at-sage>).

Nomenclature

A_c	Collector aperture area (m^2)	K	Thermal conductivity ($W m^{-1} \dot{c}K^{-1}$)
Ag	Silver	\dot{m}	Fluid mass flow rate ($kg s^{-1}$)
Al	Aluminum	MgO	Magnesium oxide
Al_2O_3	Aluminum oxide	MWCNT	Multi-walled carbon nanotubes
$AlCl_3$	Aluminum trichloride	PEG	Pentaethylene glycol
CeO_2	Cerium (IV) oxide	Q_u	Usable heat gain (W)
C_p	Fluid specific heat capacity ($kJ kg^{-1} \dot{c}K^{-1}$)	RTD	Resistance temperature detectors
Cu	Copper	SEM	Scanning electron microscope
CuO	Copper (II) oxide	SiO_2	Silicon dioxide
DMF	Dimethylformamide	SWCNTs	Single-wall carbon nanotubes
EDX	Energy-dispersive X-ray spectroscopy	T_a	Room temperature (K)
Fe_3O_4	Iron (II, III) oxide	TGr	Thermally treated graphene
FPSC	Flat-plate solar collector	THF	Tetrahydrofuran
F_R	Collector heat removal factor	T_i	Input fluid temperature (K)
GrNPs	Graphene nanoplatelets	TiO_2	Titania
GO	Graphene oxide	T_o	Output fluid temperature (K)
G_T	Heat flux intensity ($W m^{-2}$)	U_L	Overall heat loss coefficient ($W m^{-2} \dot{c}K^{-1}$)
HCl	Hydrochloric acid	WO_3	Tungsten (VI) oxide
Greek symbols			
μ	Viscosity (mPa $\dot{c}s$)	$\tau\alpha$	Transmittance-absorptance product
η_c	Collector performance	ϕ	Mass concentration (wt%)
ρ	The fluid density ($kg m^{-3}$)		

Introduction

One of the versatile solar conversion devices for residential and industrial applications is the thermal active surface (solar collector). The solar collector absorbs and converts solar energy to heat in a suitable base fluid, for example, ethylene glycol, oil, or water (H_2O).^{1–3} The flat-plate solar collector (FPSC) device consists of an absorber plate that can be made of copper (Cu) or aluminum (Au) materials and coated with a specific surface coating to increase the absorption of radiation. The header and riser pipelines are entirely connected on the outside of the absorber sheet to ensure the heat transfer fluid is appropriately circulated. A transparent sheet of glass is often used to reduce heat loss by radiation and convection. The concern about solar collectors is not only their reduced overall energy efficiency but also the limited convective heat transfer propensity of the absorbent plate and the absorbing medium.^{4,5}

One of the innovative ways to increase the performance of flat-plate collectors is to use nanofluids as working fluids,^{6–11} rather than conventional liquids. Initially, Choi and Eastman¹² suggested the use of nanofluid, defined as a colloidal mixture of solid nanoparticles (<100 nm) suspended in classical fluids. They have excellent thermophysical properties, providing an efficient heat transfer cycle, as well as more effective heat absorption compared with conventional liquids.^{13–17} Several metal nanomaterials, such as Cu, Al, and silver,^{18–20} along with various forms of metal oxides, such as copper oxide, aluminum oxide (Al_2O_3), iron oxide, and magnesium oxide, were used as additives for working fluids inside FPSCs.²¹ Due to its

extreme thermal conductivity, moderate density, and low preparation cost, Al_2O_3 - H_2O nanofluid is the most commonly used medium among other metallic oxides-based nanofluids in the FPSC. Sundar et al.²² had explored the effect of using Al_2O_3 nanofluids under a turbulent flow regime in a flat-plate collector. They measured two concentrations of nanofluid in distilled water (DW): 0.1 and 0.3 wt% of 20 nm Al_2O_3 -NPs. The twisted taped FPSC was measured at three distinct pitch ratios (H/D) of 5, 10, and 15. Also, the FPSC without the twisted tapes was tested. Their results showed that the efficiency of the FPSC with a twisted tape of $H/D = 5$ was improved by 18% compared to the FPSC with H_2O as a heat transfer fluid, for nanoparticles content of 0.3 wt% and a flow rate of $5 kg min^{-1}$.

Specific samples of crystallized semiconductor oxide nanomaterials have been used as heat exchange fluids in FPSCs, such as titanium dioxide, cerium dioxide, and tungsten trioxide.^{23–25} Despite its poor thermal conductivity, silicon dioxide (SiO_2) was also used by many researchers as a H_2O -dependent nanofluid in FPSCs. Noghrehabadi et al.²⁶ used 1 wt% SiO_2 - H_2O to investigate the laminar and turbulent flows within a square-type solar thermal system. The thermal performance of FPSC was found to increase at the specified flow rates of $0.5 kg min^{-1}$ and $2.8 kg min^{-1}$ by 1% and 2.5%, respectively.

Allotropes of carbon such as single-walled carbon nanotubes (SWCNTs), multi-walled carbon nanotubes (MWCNTs), graphene nanoplatelets (GrNPs), graphene oxide (GO), and graphene (Gr) have recently been tested as absorbing mediums rather than industrial samples inside the FPSCs.^{27–30} Said et al.^{27,31} studied the theoretical and

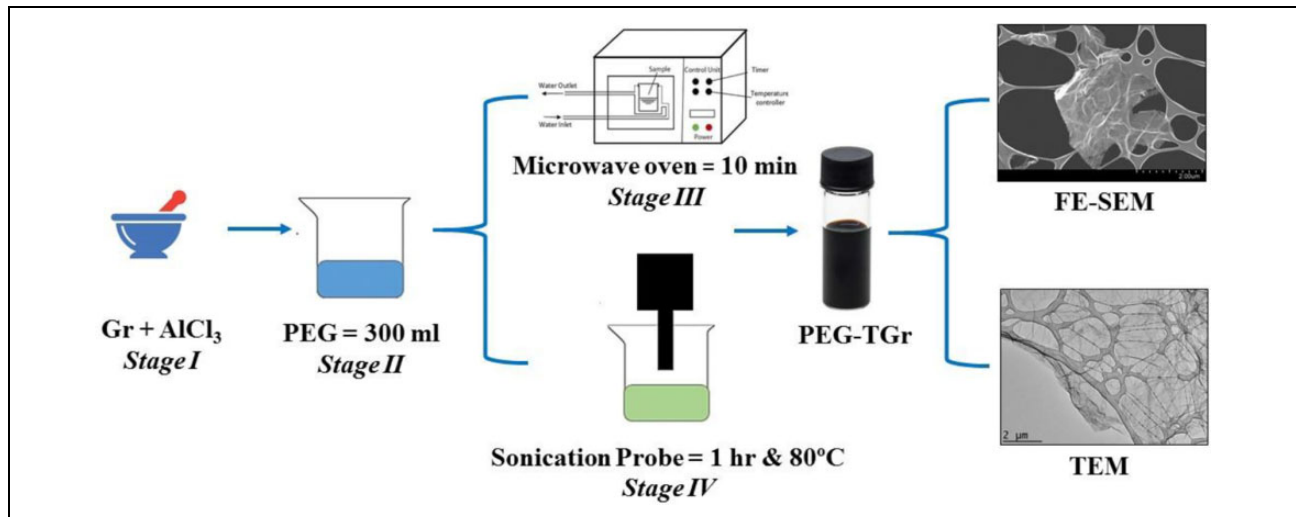


Figure 1. Schematic illustration of the acid treatment for PEG-TGr. PEG-TGr: pentaethylene glycol-thermally treated graphene.

experimental effect of using SWCNT-H₂O nanofluid on heat transport, pressure loss, and exergy performance of the solar collector. Their tests revealed that when loading 3 wt% SWCNT-H₂O at a flow rate of 0.5 kg min⁻¹, the energy and exergy performance of the system reached approximately 95% and 26.25%, respectively. Yousefi et al.³² experimentally analyzed the effectiveness implications of using MWCNT-H₂O inside a solar collector. The solar energy efficiency was found to be increased at a mass flow rate of 2 kg min⁻¹ by 28.6% for 0.2 wt% MWCNT-H₂O. The experimental effects of application GrNPs-H₂O nanofluid on the FPSC performance were studied by Vakili et al.²⁸ The study found energy efficiency improvements of up to 13.5%, 19.7%, and 23.2% for 0.0005%, 0.001%, and 0.005% of GrNPs-nanofluid mass fractions, respectively, at a flow rate of 0.9 kg min⁻¹. Ahmadi et al.³³ evaluated the effect of Gr-H₂O nanofluids on the efficiency of the FPSC theoretically and experimentally. Their conclusions exhibited that the collector energy performance was enhanced by 18.9% with 0.02 wt% Gr-H₂O at 0.9 kg min⁻¹. In recent research, Akram et al.³⁴ explored the implications of Clove-treated graphene nanoplatelet (CGNP)-H₂O for enhancing the efficacy of the FPSC. Experimental results indicated that the peak energy efficiency was obtained by using 0.1 wt% CGNP-H₂O nanofluid in the solar collector with a flow rate of 0.0260 kg s⁻¹cm⁻², which was about 18.2% higher than H₂O as working fluid for the same conditions.

Further work is required to understand the carbon-based nanofluids within the solar collector as the absorption mediums. The investigations were performed using different operating conditions such as; the working fluids were DW and aqueous nanofluids with specific mass percentages. The working fluids flowed to the FPSC system under different operating conditions such as different inlet

temperatures, heat flow densities, and fluid mass flow rates. A regression model was developed based on the collected data to estimate the thermal efficiency of FPSC.

Materials and methods

Synthesis of PEG-TGr-H₂O nanofluids

The pristine Gr in few-layer nanoparticles was supplied from the company VCN Co., Ltd, Bushehr, Iran, for nanomaterials. Different chemicals such as pentaethylene glycol (PEG; average Mn of 250, purity 90%), aluminum chloride, hydrochloric acid, *N,N*-dimethylformamide, and tetrahydrofuran were locally sourced from Sigma-Aldrich (M) Sdn. Bhd, Selangor, Malaysia. The standard protocol for experimentation is schematically shown in Figure 1. The current study followed the same chemical reactions with some changes to synthesize the nanomaterials as in the previous study.³⁵ A precision balance (OHAUS PA214) was used to measure the accurate weight of nanoparticles. An ultrasonication probe (Vibra-Cell, Sonics, VC 750) was used for dispersing the nanomaterial in the base fluid and also for preparing the covalently functionalized PEG-thermally treated graphene (PEG-TGr).

Experimental system

The experimental configuration for evaluating the energy efficiency of the indoor FPSC based Gr nanofluids is shown in Figure 2. The test rig setup included a flat-plate collector, control and measurement equipment, cooled H₂O bath, flow piping loop, and a data logger. For the movement of the working fluid, a motorized centrifugal pump was used in the forced convection system. Table 1 gives detailed specifications for the portion of the collector used in this

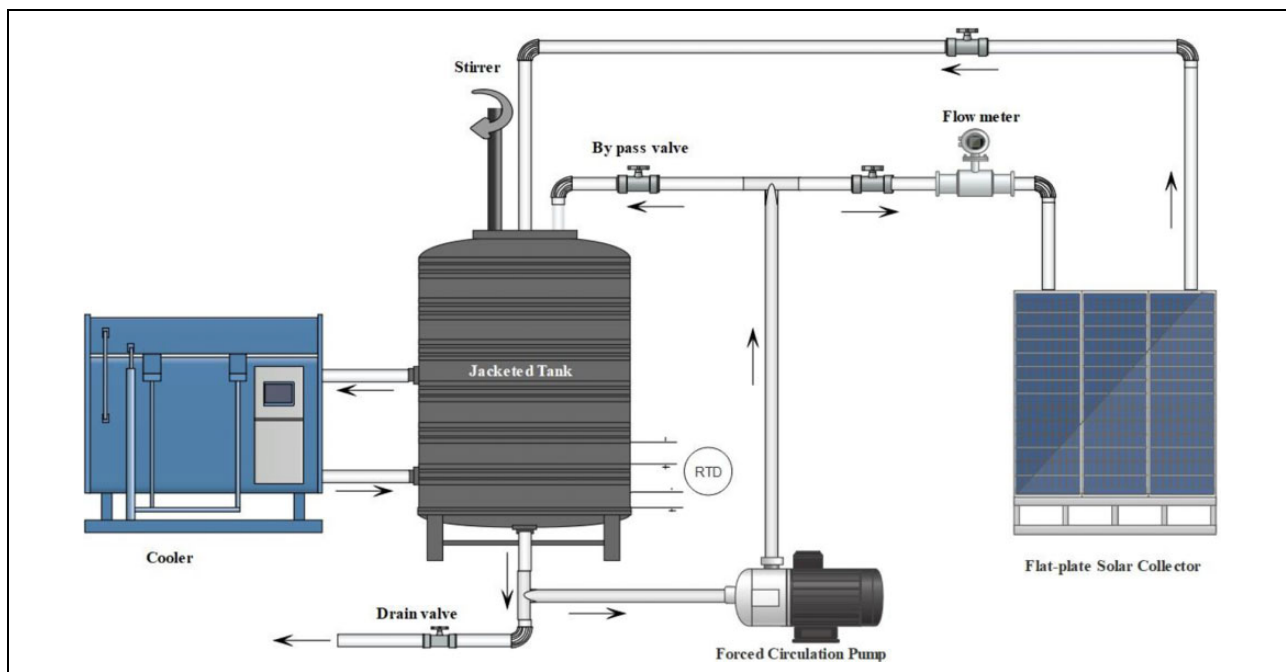


Figure 2. The schematic diagram of the thermal flat-plate collector setup.

Table 1. Technical specifications of the FPSC.

Specifications	Dimension	Unit
FPSC		
Length	1.135	m
Width	0.6	m
Thickness	0.005	m
Absorptance	0.95	–
Material	Cu	–
Area		
Collector occupied	0.681	m ²
Absorption	0.464	m ²
Header pipe		
Outer diameter	0.022	m
Inner diameter	0.0196	m
Length	0.6	m
Material	Cu	–
Riser pipe		
Outer diameter	0.0127	m
Inner diameter	0.0105	m
Length	1.02	m
Spacing	0.128	m
Material	Cu	–
Glass cover		
Thickness	0.005	m
Transmittance	0.83	–
Emissivity	0.88	–
Slope of collector		
Tilt angle	30	°

Cu: copper; FPSC: flat-plate solar collector.

research. The Cu absorber plate was soldered directly through the Cu riser tubing contact length (Figure 3). Iso-wool ceramic fiber (thermal conductivity of 0.07 W

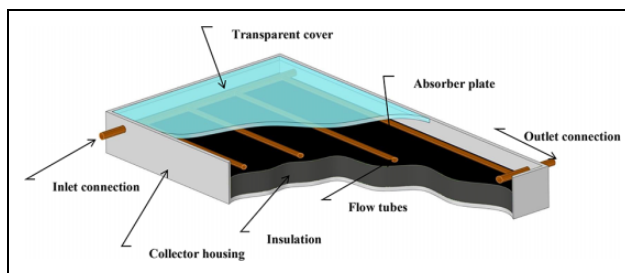


Figure 3. The main components of a FPSC. FPSC: flat-plate solar collector.

$\text{m}^{-1}\text{cK}^{-1}$ at 400°C) was used underneath the absorber plate as a high-temperature insulating sheet. The versatile adhesive heater was connected to an adjustable voltage transformer to supply the heating system with the equivalent constant heat flux. Super-fast-response self-adhesive thermocouples (T-type, model: SA1XL-T-72, Omega, USA, Omega Engineering Inc., Norwalk, Connecticut) were used to test the surface temperature of the riser tubes used in this work and the absorber plate. The 12 calibrated thermocouples were axially mounted in four separate locations along the absorber plate surface and two riser tubes. Besides, two resistance thermometers (resistance temperature detectors (RTDs); type PT100, Omega, USA) were installed at the intake and exhaust pipes to control the absorbing medium's bulk temperatures. To analyze and monitor the experimental data, an 18-channel Ecolog paperless recorder system (EC18, Kuala Lumpur, MALAYSIA.) has facilitated the connection of thermocouples and RTDs with a data logger.

Data processing and errors analysis

The useful energy (Q_u) can be determined from the equation accordingly³⁶

$$Q_u = \dot{m}C_p(T_o - T_i) \quad (1)$$

where, \dot{m} , C_p , and $T_o - T_i$ refer to the mass flow rate, the fluid specific heat capacity of nanofluids, and the difference between the output/input liquid temperature, respectively.

A further illustration of the useful energy amount is given based on the distinction between the energy absorbed, and heat loss of the system is shown below³⁶

$$Q_u = F_R A_c (G_T(\tau\alpha) - U_L(T_i - T_a)) \quad (2)$$

Therefore, F_R , A_c , G_T , $\tau\alpha$, and U_L refer to heat loss coefficient, the collector aperture area, global solar irradiation, transmittance-absorptance product, and collector heat loss coefficient related to aperture area, respectively. However $T_i - T_a$ denotes the difference between the nanofluid input/room temperatures and η_c is solar collector thermal efficiency that is generally referred to the Hottel–Whillier–Bliss equation, which is expressed as³⁶

$$\eta_c = \frac{Q_u}{A_c G_T} = \frac{\dot{m}C_p(T_o - T_i)}{A_c G_T} \quad (3)$$

$$\eta_c = F_R(\tau\alpha) - F_R U_L \frac{T_i - T_a}{G_T} \quad (4)$$

Consequently, the uncertainty in the value of FPSC efficiency calculated from the experimental data can be determined using the following relation³³

$$\frac{\partial \eta_c}{\eta_c} = \left[\left(\frac{\partial \dot{m}}{\dot{m}} \right)^2 + \left(\frac{\partial C_p}{C_p} \right)^2 + \left(\frac{\partial G_T}{G_T} \right)^2 + \left(\frac{\partial A_c}{A_c} \right)^2 + \left(\frac{\partial (T_o - T_i)}{(T_o - T_i)} \right)^2 \right]^{0.5} \quad (5)$$

Ranges and accuracies of instruments and fluid properties were shown in Table 2. The total uncertainty in the overall efficiency of the process is approximately 3.37% after the measurement procedure.

Thermophysical and characterization properties

The thermal conductivities of nanofluids and base fluid samples were calculated using a thermal analyzer (model: KD2 Pro, Decagon, Pullman, WA, USA). An average of 16 readings was obtained over 4 h for each temperature setting to determine the dispersal stability of the nanofluids. The MCR 302 Rheometer (Anton Paar, Austria) was employed for testing the dynamic viscosity of H₂O and PEG-TGr-H₂O nanofluids. Density meter Easy-D40, Mettler Toledo, Ohio, United States. was utilized for the density measurements of liquid samples with an accuracy of $\pm 10^{-4}$ g cm⁻³. For accuracy and reliability considerations, measures were taken at least three times per sample at each temperature. DSC 8000-PerkinElmer estimated the fluids specific heat

Table 2. List of ranges and accuracies for instruments and fluid properties.

Instrument and sensor type	Range	Uncertainty (%)
Type-T thermocouple	0–300°C	$\pm 0.1^\circ\text{C}$
RTD (PT100) sensor	0–200°C	$\pm 0.1^\circ\text{C}$
Burkert flow meter (Type SE32, Bürkert, Ingelfingen, Germany)	0.3–8 l min ⁻¹	$\pm 1\%$
Power supply (AC clamp meter, Kyoritsu, Tokyo, Japan)	200/600 V 200/600 A	± 1 ± 1.5
Thermal conductivity KD2 pro (Decagon)	0.2–2 W m ⁻¹ °K ⁻¹	± 5
Dynamic viscosity (Physica, MCR 302, Anton Paar)	–150 °C to +1000°C	± 1
Density Mettler Toledo (DE-40, Ohio, United States)	0–3 g cm ⁻³	± 1
Specific heat (DSC 8000, PerkinElmer, Massachusetts, United States)	0.01–300°C min ⁻¹	± 2

RTD: resistance temperature detector.

with an accuracy of $\pm 1.0\%$. Scanning electron microscope (SEM, Tescan VEGA3, Czechia) was utilized for the morphology and elemental study of functionalized synthesized powders.

Results and discussion

Morphological and thermophysical properties

A visual analysis of GrNPs surface using SEM to the identification of contaminants or unknown particles, the cause of failure and interactions between materials is shown in Figure 4(a) and (b). In addition to surface evaluation, SEM analysis is utilized for particle characterization. The high magnification, high-resolution imaging of our SEM analysis supports the determination of the number, size, and morphology of Gr particles. The surfactant-stabilized nanofluids were deposited on a silicon (Si) wafer to obtain the SEM micrographs and distributions. Also, Figure 4 shows that nanoparticles do not have an agglomeration, so they have appeared in an aggregation mechanism and are well distributed. SEM micrographs also reveal that the covalent synthesizing of Gr allows the wrinkled structures actively. Energy-dispersive X-ray spectroscopy (EDX) provides further understanding of the surface of Gr during the SEM analysis process. EDX analysis is used to acquire the elemental composition of a sample and allows for a more quantitative result than that provided by only SEM analysis. The combination of SEM and EDX analysis offers chemical composition and elemental investigation—providing a comprehensive metallurgical evaluation. The spectrum study of GrNPs with

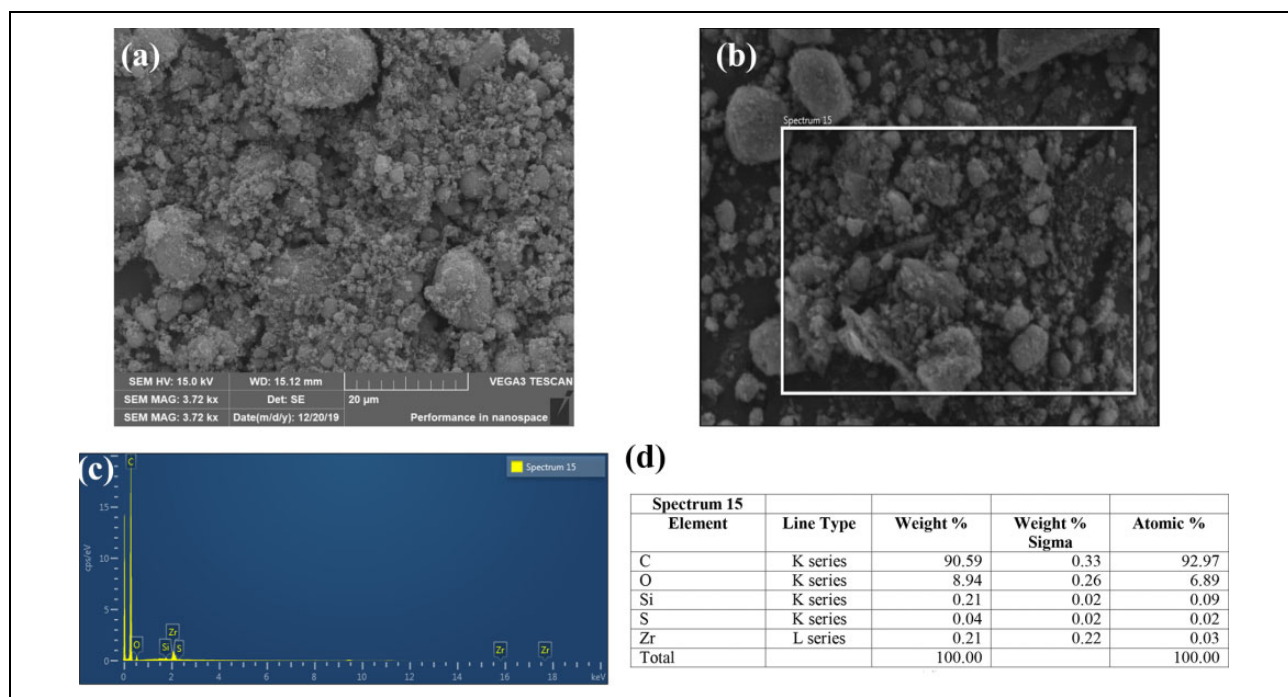


Figure 4. SEM and EDX mapping analysis of the Gr nanoparticles: (a) SEM microimage, (b) electron image of spectrum 15, (c) EDX mapping analysis, and (d) EDX elemental analysis. SEM: scanning electron microscopy; EDX: energy-dispersive X-ray spectroscopy; Gr: graphene.

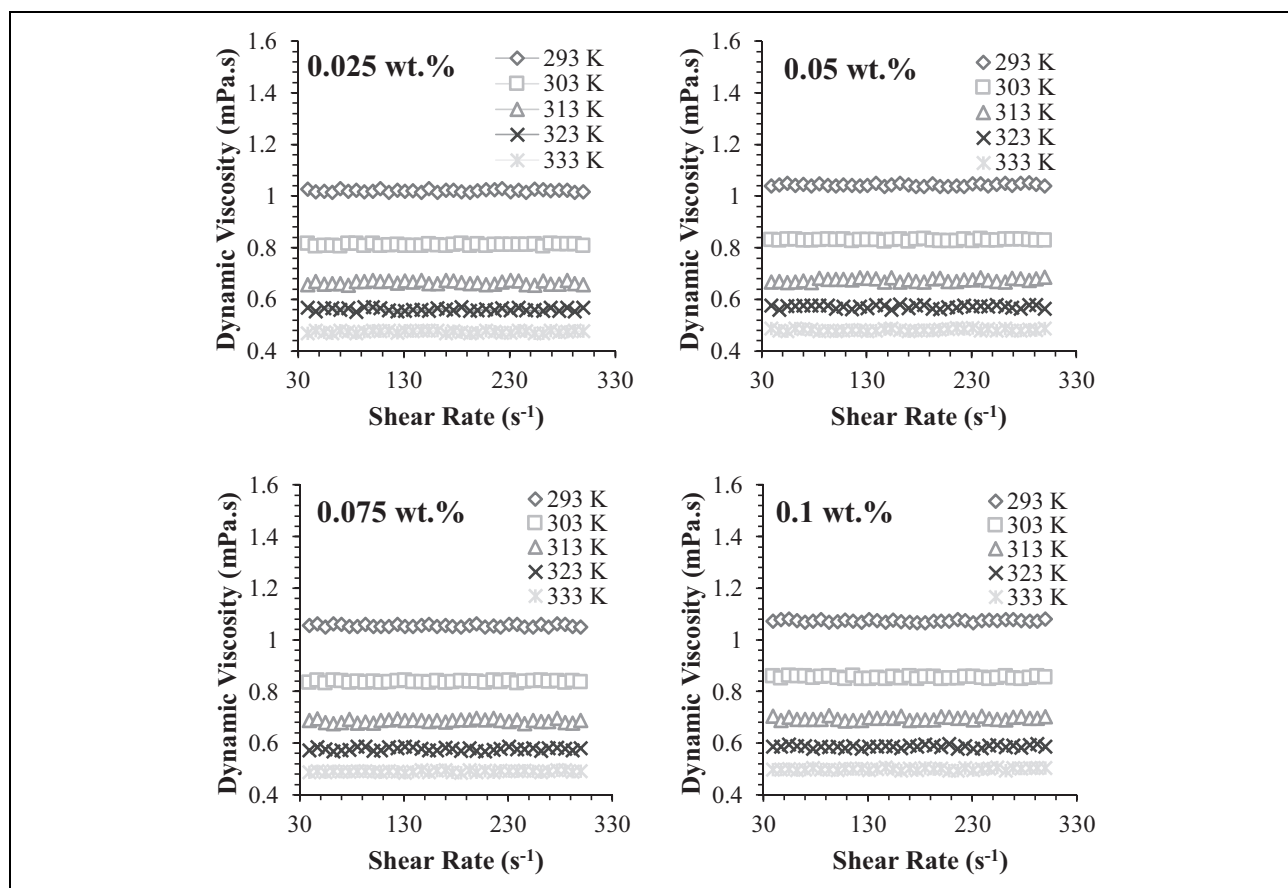


Figure 5. The measured values of dynamic viscosity against shear rate for PEG-TGr nanofluids at different temperatures and mass fractions.³⁷ PEG-TGr: pentaethylene glycol-thermally treated graphene.

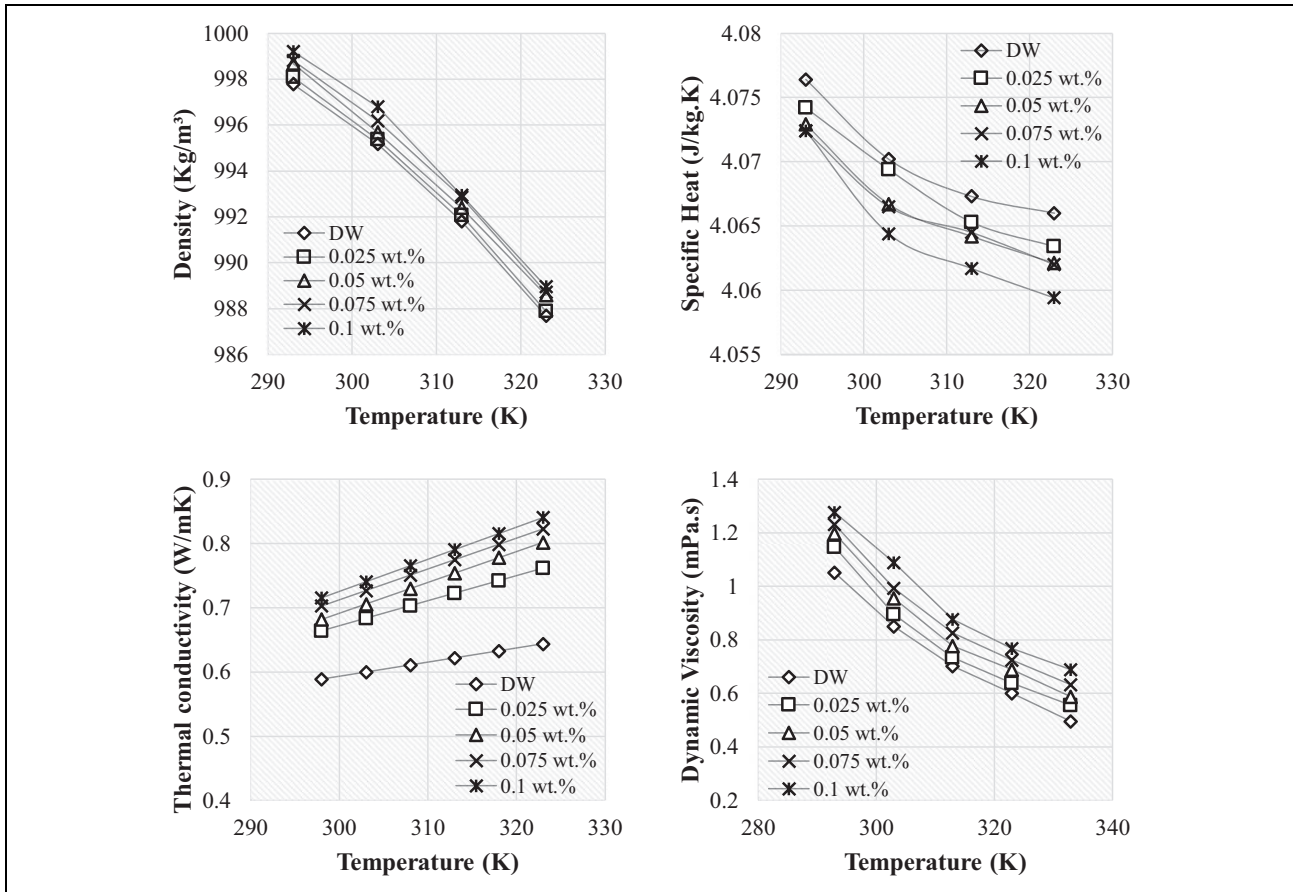


Figure 6. Thermophysical properties for DW and PEG-TGr nanofluids at different temperatures and mass fractions.³⁷ DW: distilled water; PEG-TGr: pentaethylene glycol-thermally treated graphene.

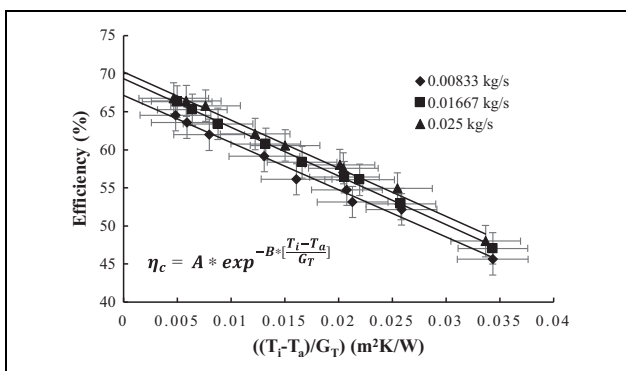


Figure 7. The experimental values of the collector efficiency for DW against the reduced temperature coefficient at different fluid mass flow rates. DW: distilled water.

EDX is shown in Figure 4(c) and (d). The EDX measurements show five elements, such as carbon, oxygen, Si, sulfur (S), and zirconium (Zr). GrNPs show a carbon content of 92.97% and an atomic oxygen content of 6.89%. While the atomic content of Si, S, and Zr is 0.09%, 0.02% and 0.03%, respectively.

The measured values of viscosity are plotted in Figure 5 as a function of shear rate for H₂O-based PEG-TGr nanofluids at different temperatures and weight concentrations. From the figure, it was observed that viscosity increases as weight concentration increases and decreases as temperature increases. Furthermore, it can also be found that the behavior of H₂O-based PEG-TGr nanofluids was quite Newtonian with almost constant viscosity with different values of shear rate. Figure 6 presents the results of thermal conductivity, dynamic viscosity, density, and specific heat capacity for base H₂O and PEG-TGr-nanofluids.^{37–39} Measurements of thermophysical properties were performed at different temperatures testing of 303, 313, and 323 K. The data collected showed that the density, dynamic viscosity, and thermal conductivity were improved by increasing the nanoparticles mass percentage in the DW, but the specific heat capacity was reduced. The maximum thermal conductivity increase value was 30.48% compared with H₂O at 323 K. Whereas an increase in viscosity of 27.53% was observed at a temperature of 303 K for the 0.1 wt% PEG-TGr-NPs. Just 0.1% was the most significant increase in density measurements. The real heat nanofluids, however, dropped by 2.9% at 0.1 wt% PEG-TGr-NPs.

Table 3. Heat gain and heat loss coefficients at different PEG-TGr-NPs mass fractions and varying flow rates.

Fluid	Mass flow rate (kg s ⁻¹)	$F_R(\tau\alpha)$	$F_R U_L$	R^2
DW	0.00833	0.671	11.273	0.989
	0.01667	0.693	10.862	0.9966
	0.025	0.702	10.187	0.992
0.025 wt%	0.00833	0.714	11.533	0.9942
	0.01667	0.736	10.889	0.9942
	0.025	0.756	10.333	0.9942
0.05 wt%	0.00833	0.728	11.831	0.9944
	0.01667	0.751	10.985	0.9944
	0.025	0.772	10.524	0.9944
0.075 wt%	0.00833	0.736	12.211	0.9982
	0.01667	0.759	11.147	0.9982
	0.025	0.780	10.643	0.9982
0.1 wt%	0.00833	0.742	12.532	0.9954
	0.01667	0.766	11.238	0.9954
	0.025	0.787	10.839	0.9954

PEG-TGr-NPs: pentaethylene glycol-thermally treated graphene nanoplatelets; DW: distilled water.

Analysis of thermal efficiency using H₂O

Initially, the working fluid (DW) flowed inside the collector setup to verify the validity, reliability, and readability of the test section results before the nanofluids were conducted in the next phase. It is observed that the data reproduced well, test rig was highly accurate and remains within an error of <1%. Figure 7 exhibits the collected data of H₂O run for the FPSC performance under the operating settings of different H₂O mass flow rates versus the lowered temperature factor ($(T_i - T_a)/G_T$). After flowing more H₂O to the system (0.01667–0.025 kg s⁻¹), the FPSC efficiency showed an increment by about 2.75% and 3.44%, respectively. The explanation for increasing the FPSC efficiency was due to the improved H₂O flow rate (H₂O mass flow rate), reduction of flat-plate surface temperature, and minimization of the overall heat loss. The coefficients of the heat gain ($F_R(\tau\alpha)$) and heat loss ($F_R U_L$) for the working fluid of H₂O are listed in Table 3. Table 3 demonstrates that the $F_R(\tau\alpha)$ value of the collector was highest when the H₂O was flowing at 0.025 kg s⁻¹, whereas the $F_R U_L$ value was lowest for the same situation. Therefore, based upon equation (4), FPSC performance can be maximized at the highest flow rates.

Analysis of thermal efficiency using nanofluids

Figure 8(a) to (c) shows the measured values of FPSC efficiency for H₂O and PEG-TGr-NPs nanofluids against the lowered temperature factor ($(T_i - T_a)/G_T$) under the operating conditions of different PEG-TGr-NPs concentrations and changed fluid mass flow rates. From Figure 8, it can be concluded that by using H₂O-suspended PEG-TGr-NPs for any concentration, the thermal performance was enhanced. As the fluid flow rate of circulating nanofluid

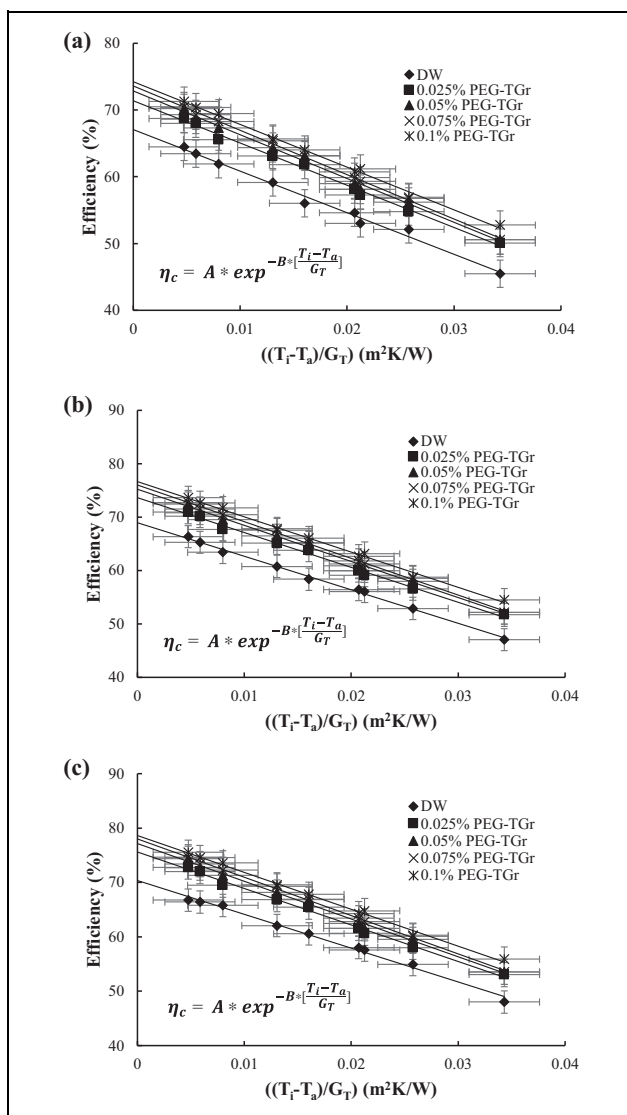


Figure 8. Thermal efficiency for H₂O and PEG-TGr-H₂O nanofluids at different mass fractions: (a) 0.00833 kg s⁻¹, (b) 0.01667 kg s⁻¹, and (c) 0.025 kg s⁻¹. H₂O: water; PEG-TGr: pentaethylene glycol-thermally treated graphene.

varies from 0.00833 kg s⁻¹, 0.01667 kg s⁻¹, and 0.025 kg s⁻¹, the FPSC efficiency was improved up to 10.6%, 11%, and 13.1%, respectively. Figure 9(a) to (d) exhibits the influence of PEG-TGr-NPs against the FPSC performance at four different weight concentrations (0.025, 0.05, 0.075 and 0.1% by mass) under the similar condition of fluid mass flow rate (0.00833, 0.01667 and 0.025 kg s⁻¹). As can be seen from Figures 8 and 9, the FPSC thermal performance enhanced when the flowing of PEG-TGr-nanofluid was increased from 0.00833 kg s⁻¹ to 0.025 kg s⁻¹ for all the employed samples. The highest increment in the FPSC energy performance corresponding to the reduced temperature parameter was about 13.1% for the testing conditions of 0.1 wt% PEG-TGr loading and fluid flow rate of

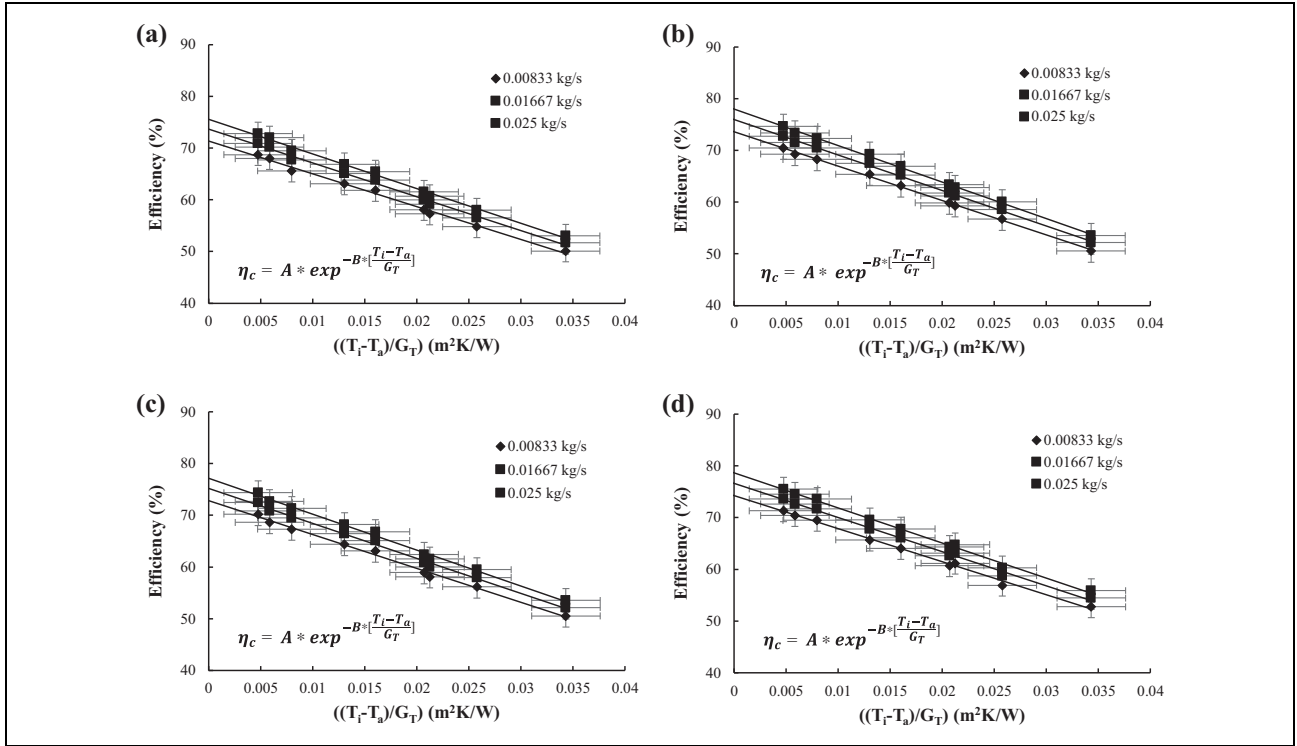


Figure 9. Thermal efficiency for PEG-TGr-H₂O nanofluids at different fluid mass flow rates: (a) 0.025 wt%, (b) 0.05 wt%, (c) 0.075 wt%, and (d) 0.1 wt%. H₂O: water; PEG-TGr: pentaethylene glycol-thermally treated graphene.

0.025 kg s⁻¹. The current research findings are consistent with preceding studies by Vakili et al.²⁸ and Karami et al.⁴⁰ It was also found that higher PEG-TGr weight fractions contributed to higher input energy absorption, hence resulting in an improvement in the FPSC effectiveness. The heat was distributed evenly across the fluid layers for the low content of Gr nanoparticles; the heat loss at the flow boundary is much lower for the lower concentration of PEG-TGr compared to the higher nanofluid weight fraction in which the uppermost fluid layers are dominated by more heat absorption. This high-temperature region at the wall boundary contributes more spaces for heat losses, thereby decreasing the effectiveness of the collector. Table 4 compares the previous experimental data on using carbon-based nanofluids inside the FPSCs.

The critical factor for improving the FPSC effectiveness by introducing PEG-TGr nanopowder into the base fluid can be described by the following: the specific heat capacity of the nanofluids (Cp_{nf}) to be evaluated is slightly lower than (Cp_{bf}) but the temperature distinction produced by the nanofluids ($T_o - T_i$) is significantly higher than that by the base fluid. A substantial increase in the experimental thermal efficiency has then resulted from the combination of the above two conditions.^{48–50}

Table 3 and Figure 10(a) and (b) below illustrate the $F_R(\tau\alpha)$ and $F_R U_L$ for PEG-TGr-DW nanofluids. When the nanofluid flows at a constant flow rate (0.00833 kg s⁻¹) and varied Gr weight concentrations (0.025 wt%, 0.05 wt%,

0.075 wt%, and 0.1 wt%), $F_R(\tau\alpha)$ values progressively increased by 6.28%, 8.49%, 9.68%, and 10.53%, respectively, relative to the data of base fluid. The heat absorption factors also showed upward trends for 0.01667 kg s⁻¹ flow rate at 0.025 wt%, 0.05 wt%, 0.075 wt%, and 0.1 wt% PEG-TGr concentrations by up to 6.25%, 8.39%, 9.54%, and 10.53%, respectively. Meanwhile, given a flow rate of the fluid at 0.025 kg s⁻¹, there was an enhancement for ($F_R(\tau\alpha)$) by 7.63%, 9.90%, 11.04%, and 12.01%, respectively, for 0.025 wt%, 0.05 wt%, 0.075 wt%, and 0.1 wt% PEG-TGr nanofluids. When flow rate was at the lower range (0.00833 kg s⁻¹), the corresponding value of $F_R U_L$ for 0.025 wt%, 0.05 wt%, 0.075 wt%, and 0.1 wt% PEG-TGr concentrations had increased by 2.31%, 4.95%, 8.32%, and 11.17%. Meanwhile, at higher fluid mass flow rate (0.025 kg s⁻¹), the $F_R U_L$ value incremented by 1.43%, 3.31%, 4.48%, and 6.40% for different concentrations as used in the present work.

Proposed model of thermal efficiency

New thermal efficiency correlation was developed as a function of the reduced temperature factor ($(T_i - T_a)/G_T$) (equation 6). An exponential form was used to derive the FPSC thermal effectiveness based on the experimental data with statistical significance at a confidence level of 95%. A maximum deviation of about 6.782%, standard deviation of about 1.962%, and average deviation of about 4.485% were

Table 4. Previous experimental studies on the use of carbon nanofluids in FPSCs.

References	Nanoparticles					Solar collector	Remarks
	Base fluid	Type	Size (nm)	Concentration	Surfactant		
21	H ₂ O	MWCNTs	—	0.1–0.3 vol%	Triton X-100	—	Maximum collector effectiveness of 30.58%. Energy efficiency improved by 95.12% for 0.3 vol% and 0.5 kg min ⁻¹ .
27	H ₂ O	SWCNTs	1–2	0.1–0.3 vol%	SDS	1.84 m ²	
32	H ₂ O	MWCNTs	10–30	0.2–0.4 wt%	Triton X-100	1.51 m ²	The efficiency of 0.4 wt% MWCNT was higher than for H ₂ O.
33	H ₂ O	GrNPs	—	0.01–0.2 wt%	—	$0.47 \times 0.27 \times 0.001 \text{ m}^3$	Thermal efficiency up to 18.87%.
41	H ₂ O	MWCNTs	10–30	0.2 wt%	Triton X-100	1.51 m ²	F_{RUL} was more influential at high temperature gradients.
42	H ₂ O	MWCNTs	10–12	0.15–1 vol%	—	$L = 0.51 \text{ m}, t = 0.001 \text{ m}$	Maximum instantaneous efficiency was 73% at 0.6 vol%.
43	H ₂ O	MWCNTs	10–12	—	—	—	This analysis examined the effects of different filling ratios (50%, 60%, and 70%).
44	H ₂ O	Gr, MWCNTs, CuO, Al ₂ O ₃ , TiO ₂ , SiO ₂	20, 7, 42, 45, 44, 10	0.25–2 vol%	Triton 100-X	0.375 m ²	Maximum exergetic and energetic efficiencies of MWCNTs were 29.32% and 23.47%.
45	H ₂ O	PEG-GrNPs	—	0.025–0.1 wt%	—	0.464 m ²	The maximum efficiency increase was about 13.3% at 0.025 kg s ⁻¹ .
46	H ₂ O	TEA-GrNPs	—	0.025–0.1 wt%	—	914.4 x 508.0 mm ²	As wt% of TEA-GrNPs increased, efficiency improved up to 10.53%.
47	H ₂ O	MWCNTs-GrNPs- h-BN	—	0.05, 0.08, and 0.1 wt%	Tween-80	1.92 m ²	Hybrid nanofluid improves the efficiency by about 20% higher than DW.
Current study	H ₂ O	PEG-TGr	—	0.025–0.1 wt%	—	0.464 m ²	The maximum efficiency increase was about 13.1% at 0.025 kg s ⁻¹ .

CuO: copper oxide; TiO₂: titanium dioxide; SiO₂: silicon dioxide; GrNP: graphene nanoplatelet; FPSC: flat-plate solar collector; h-BN: Boron nitride; H₂O: water; TEA: Triethanolamine; MWCNT: multi-walled carbon nanotube; SDS: Sodium dodecyl sulfate; SWCNT: single-walled carbon nanotube; Gr: graphene; Al₂O₃: aluminum oxide; PEG-TGr: pentaethylene glycol-thermally treated graphene.

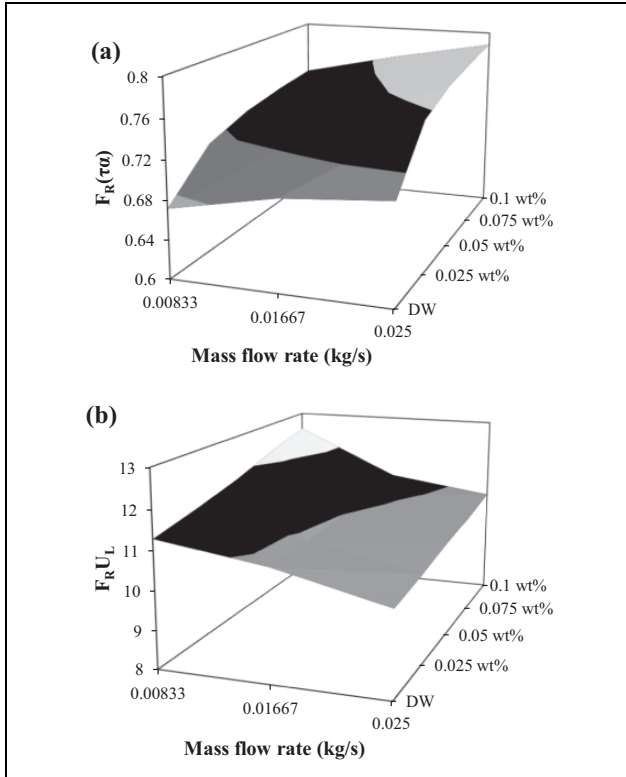


Figure 10. (a) The heat gain coefficient ($F_R(\tau\alpha)$) and (b) the heat loss coefficient ($F_R U_L$) for H_2O and PEG-TGr- H_2O nanofluids as a function of mass fraction and mass flow rate. H_2O : water; PEG-TGr: pentaethylene glycol-thermally treated graphene.

Table 5. The coefficients of the developed correlations for the FPSC efficiency based H_2O and nanofluids at different mass flow rates.

Mass flow rate ($kg\ s^{-1}$)	Sample (wt%)	A	B	R^2
0.00833	DW	68.073	11.2	0.9868
	0.025	72.245	10.64	0.9953
	0.05	73.795	10.84	0.9936
	0.075	74.655	10.93	0.9932
	0.1	75.13	10.29	0.9952
0.01667	DW	70.415	11.25	0.9913
	0.025	74.563	10.64	0.9953
	0.05	76.162	10.84	0.9936
	0.075	77.05	10.93	0.9932
	0.1	77.54	10.29	0.9952
0.025	DW	71.195	10.91	0.9823
	0.025	76.521	10.64	0.9953
	0.05	78.162	10.84	0.9936
	0.075	79.073	10.93	0.9932
	0.1	79.576	10.29	0.9952

FPSC: flat-plate solar collector; DW: distilled water; H_2O : water.

observed between the experimental and proposed correlation values for all the nanofluids examined. The coefficients of the new correlation are presented in Table 5 along with R^2 values.

$$\eta_c = A \times \exp^{-B \times \left[\frac{T_i - T_a}{G_T} \right]} \quad (6)$$

Conclusions

The current research aimed to experimentally discuss the impact of using few-layer Gr in aqueous suspensions as the absorbing medium on the FPSC energy efficiency. Different variables were considered during the investigations, such as various weight concentrations, different fluid flowing rates, different input fluid temperatures, and different input heat rates. After the discussion of the results aforementioned, the following conclusions were drawn;

1. The EDX measurements portray two components present in CF-GrNPs; carbon and oxygen. Si, S, and Zr were present as a result of the oxidizing agent and from the substrate. The best enhancements in the thermophysical properties of PEG-TGr-DW relative to the base fluid were recorded as 30.48% for thermal conductivity at 323 K and 27.53% for dynamic viscosity at 0.1 wt% PEG-TGr and 303 K. The measured density with the maximum concentration value had an increment of 0.1%, whereas the specific heat reduced to 2.9% for the same concentration of 0.1 wt% PEG-TGr- H_2O .
2. Improvements in the FPSC energy efficiency relied on increases in heat flux intensity and nanofluid mass flowing rate of PEG-TGr. A reduction in thermal energy was reported as the nanofluid input temperature was raised. For the measured mass flowing rates of 0.00833, 0.01667, and 0.025 $kg\ s^{-1}$, the highest collector performance increases are 10.6%, 11%, and 13.1%, respectively, with 0.1 wt% nanofluid.
3. The highest observed increment in the heat loss coefficient ($F_R U_L$) and the *heat gain coefficient* ($F_R(\tau\alpha)$) was 11.17% and 12.01%, respectively, for 0.1 wt% PEG-TGr concentration at 0.00833 and 0.025 $kg\ s^{-1}$ mass flow rates.
4. New thermal efficiency correlation was developed as a function of the reduced temperature factor ($(T_i - T_a)/G_T$).

Acknowledgment

The authors gratefully acknowledge the financial support from Universiti Teknologi Malaysia, operated by the Research Management Center (RMC).


Declaration of conflicting interests

The author(s) declared no potential conflicts of interest with respect to the research, authorship, and/or publication of this article.

Funding

The author(s) disclosed receipt of the following financial support for the research, authorship, and/or publication of this article: This work was supported by the Universiti Teknologi Malaysia, operated by the Research Management Center (RMC), under the Research University grant number 04E76.

ORCID iD

Omer A Alawi  <https://orcid.org/0000-0002-8598-4461>

References

1. Khodabandeh E, Safaei MR, Akbari S, et al. Application of nanofluid to improve the thermal performance of horizontal spiral coil utilized in solar ponds: geometric study. *Renew Energy* 2018; 122: 1–16.
2. Mallah AR, Mohd Zubir MN, Alawi OA, et al. Plasmonic nanofluids for high photothermal conversion efficiency in direct absorption solar collectors: fundamentals and applications. *Sol Energy Mater Sol Cells* 2019; 201: 110084.
3. Sarafraz MM, Tlili I, Tian Z, et al. Smart optimization of a thermosyphon heat pipe for an evacuated tube solar collector using response surface methodology (RSM). *Phys A Stat Mech Appl* 2019; 534: 122146.
4. Raj P and Subudhi S. A review of studies using nanofluids in flat-plate and direct absorption solar collectors. *Renew Sust Energy Rev* 2018; 84: 54–74.
5. Goshayeshi HR and Safaei MR. Effect of absorber plate surface shape and glass cover inclination angle on the performance of a passive solar still. *Int J Numer Methods Heat Fluid Flow* 2019; 30(6): 3183–3198.
6. Olia H, Torabi M, Bahiraei M, et al. Application of nanofluids in thermal performance enhancement of parabolic trough solar collector: state-of-the-art. *Appl Sci* 2019; 9: 463.
7. Sarafraz MM and Safaei MR. Diurnal thermal evaluation of an evacuated tube solar collector (ETSC) charged with graphene nanoplatelets-methanol nano-suspension. *Renew Energy* 2019; 142: 364–372.
8. Sarafraz MM, Tlili I, Baseer MA, et al. Potential of solar collectors for clean thermal energy production in smart cities using nanofluids: experimental assessment and efficiency improvement. *Appl Sci* 2019; 9(9): 1877.
9. Sarafraz MM, Tlili I, Tian Z, et al. Thermal evaluation of graphene nanoplatelets nanofluid in a fast-responding HP with the potential use in solar systems in smart cities. *Appl Sci* 2019; 9(10): 2101.
10. Peng Y, Zahedastjerdi A, Abdollahi A, et al. Investigation of energy performance in a U-shaped evacuated solar tube collector using oxide added nanoparticles through the emitter, absorber and transmittal environments via discrete ordinates radiation method. *J Therm Anal Calorim* 2020; 139(4): 2623–2631.
11. Zhou X, Wang Y, Zheng K, et al. Comparison of heat transfer performance of ZnO-PG, α -Al₂O₃-PG, and γ -Al₂O₃-PG nanofluids in car radiator. *Nanomater Nanotechnol* 2019; 9: 1847980419876465.
12. Choi SUS and Eastman JA. Enhancing thermal conductivity of fluids with nanoparticles. *ASME Int Mech Eng Congr Expo* 1995; 66: 99–105.
13. Sakhaei SA and Valipour MS. Performance enhancement analysis of the flat plate collectors: a comprehensive review. *Renew Sust Energy Rev* 2019; 102: 186–204.
14. Yarmand H, Gharekhani S, Shirazi SFS, et al. Study of synthesis, stability and thermo-physical properties of graphene nanoplatelet/platinum hybrid nanofluid. *Int Commun Heat Mass Transf* 2016; 77: 15–21.
15. Liu WI, Malekhamadi O, Bagherzadeh SA, et al. A novel comprehensive experimental study concerned graphene oxide nanoparticles dispersed in water: synthesise, characterisation, thermal conductivity measurement and present a new approach of RLSF neural network. *Int Commun Heat Mass Transf* 2019; 109: 104333.
16. Safaei MR, Ahmadi G, Goodarzi MS, et al. Heat transfer and pressure drop in fully developed turbulent flows of graphene nanoplatelets-silver/water nanofluids. *Fluids* 2016; 1(20): 1–2.
17. Bahiraei M, Mazaheri N, Aliee F, et al. Thermo-hydraulic performance of a biological nanofluid containing graphene nanoplatelets within a tube enhanced with rotating twisted tape. *Powder Technol* 2019; 355: 278–288.
18. Zayed ME, Zhao J, Du Y, et al. Factors affecting the thermal performance of the flat plate solar collector using nanofluids: a review. *Sol Energy* 2019; 182: 382–396.
19. He Q, Zeng S, and Wang S. Experimental investigation on the efficiency of flat-plate solar collectors with nanofluids. *Appl Therm Eng* 2014; 88: 165–171.
20. Tomy AM, Ahammed N, Subathra MSP, et al. Analysing the performance of a flat plate solar collector with silver/water nanofluid using artificial neural network. *Procedia Comput Sci* 2016; 93: 33–40.
21. Rajput NS, Shukla DDB, and Sharma SK. Thermal analysis of MWCNT/distilled water nanofluid on the efficiency of flat plate solar collector. *Int J Mech Eng Technol* 2017; 8: 233–240.
22. Sundar LS, Singh MK, Punnaiah V, et al. Experimental investigation of Al₂O₃/water nanofluids on the effectiveness of solar flat-plate collectors with and without twisted tape inserts. *Renew Energy* 2018; 119: 820–833.
23. Kiliç F, Menlik T, and Sözen A. Effect of titanium dioxide/water nanofluid use on thermal performance of the flat plate solar collector. *Sol Energy* 2018; 164: 101–108.
24. Sharafeldin MA, Gróf G, and Mahian O. Experimental study on the performance of a flat-plate collector using WO₃/water nanofluids. *Energy* 2017; 141: 2436–2444.
25. Sharafeldin MA and Gróf G. Experimental investigation of flat plate solar collector using CeO₂-water nanofluid. *Energy Convers Manag* 2018; 155: 32–41.
26. Noghrehabadi A, Hajidavaloo E, and Moravej M. Experimental investigation of efficiency of square flat-plate solar collector using SiO₂/water nanofluid. *Case Stud Therm Eng* 2016; 8: 378–386.

27. Said Z, Saidur R, Sabiha MA, et al. Thermophysical properties of single wall carbon nanotubes and its effect on exergy efficiency of a flat plate solar collector. *Sol Energy* 2015; 115: 757–769.
28. Vakili M, Hosseinalipour SM, Delfani S, et al. Experimental investigation of graphene nanoplatelets nanofluid-based volumetric solar collector for domestic hot water systems. *Sol Energy* 2016; 131: 119–130.
29. Vincely DA and Natarajan E. Experimental investigation of the solar FPC performance using graphene oxide nanofluid under forced circulation. *Energy Convers Manag* 2016; 117: 1–11.
30. Safaei MR, Goshayeshi HR, and Chaer I. Solar still efficiency enhancement by using graphene oxide/paraffin nano-PCM. *Energies* 2019; 12(10): 2002.
31. Said Z, Saidur R, Rahim NA, et al. Analyses of exergy efficiency and pumping power for a conventional flat plate solar collector using SWCNTs based nanofluid. *Energy Build* 2014; 78: 1–9.
32. Yousefi T, Veisy F, Shojaeizadeh E, et al. An experimental investigation on the effect of MWCNT-H₂O nanofluid on the efficiency of flat-plate solar collectors. *Exp Therm Fluid Sci* 2012; 39: 207–212.
33. Ahmadi A, Ganji DD, and Jafarkazemi F. Analysis of utilizing graphene nanoplatelets to enhance thermal performance of flat plate solar collectors. *Energy Convers Manag* 2016; 126: 1–11.
34. Akram N, Sadri R, Kazi SN, et al. An experimental investigation on the performance of a flat-plate solar collector using eco-friendly treated graphene nanoplatelets–water nanofluids. *J Therm Anal Calorim* 2019; 138(1): 609–621.
35. Alawi OA, Sidik NAC, Kazi SN, et al. Graphene nanoplatelets and few-layer graphene studies in thermo-physical properties and particle characterization. *J Therm Anal Calorim* 2019; 135(2): 1081–1093.
36. Hawwash AA, Abdel Rahman AK, Nada SA, et al. Numerical investigation and experimental verification of performance enhancement of flat plate solar collector using nanofluids. *Appl Therm Eng* 2018; 130: 363–374.
37. Alawi OA, Mallah AR, Kazi SN, et al. Thermophysical properties and stability of carbon nanostructures and metallic oxides nanofluids: experimental approach. *J Therm Anal Calorim* 2019; 135(2): 1545–1562.
38. Goodarzi M, Kherbeet AS, Afrand M, et al. Investigation of heat transfer performance and friction factor of a counter-flow double-pipe heat exchanger using nitrogen-doped, graphene-based nanofluids. *Int Commun Heat Mass Transf* 2016; 76: 16–23.
39. Maithani R, Kumar A, Gholamali Zadeh P, et al. Empirical correlations development for heat transfer and friction factor of a solar rectangular air passage with spherical-shaped turbulence promoters. *J Therm Anal Calorim* 2020; 139(2): 1195–1212.
40. Karami M, Akhavan-Behabadi MA, Dehkordi MR, et al. Thermo-optical properties of copper oxide nanofluids for direct absorption of solar radiation. *Sol Energy Mater Sol Cells* 2016; 144: 136–142.
41. Yousefi T, Shojaeizadeh E, Veysi F, et al. An experimental investigation on the effect of pH variation of MWCNT–H₂O nanofluid on the efficiency of a flat-plate solar collector. *Sol Energy* 2012; 86: 771–779.
42. Chougule SS, Sahu SK, and Pise AT. Thermal performance of two phase thermosyphon flat-plate solar collectors using nanofluid. *J Sol Energy Eng* 2014; 136: 14503.
43. Chougule SS and Sahu SK. Performance of carbon nanotubes–water nanofluid charged wickless heat pipe flat plate solar collectors having different filling ratio. *J Sol Energy Eng* 2015; 137: 24501.
44. Verma SK, Tiwari AK, and Chauhan DS. Experimental evaluation of flat plate solar collector using nanofluids. *Energy Convers Manag* 2017; 134: 103–115.
45. Alawi OA, Mohamed Kamar H, Mallah AR, et al. Thermal efficiency of a flat-plate solar collector filled with pentaethylene glycol-treated graphene nanoplatelets: an experimental analysis. *Sol Energy* 2019; 191: 360–370.
46. Sarsam WS, Kazi SN, and Badarudin A. Thermal performance of a flat-plate solar collector using aqueous colloidal dispersions of graphene nanoplatelets with different specific surface areas. *Appl Therm Eng* 2020; 172: 115142.
47. Hussein OA, Habib K, Muhsan AS, et al. Thermal performance enhancement of a flat plate solar collector using hybrid nanofluid. *Sol Energy* 2020; 204: 208–222.
48. Sarafraz MM, Safaei MR, Tian Z, et al. Thermal assessment of nano-particulate graphene-water/ethylene glycol (WEG 60:40) nano-suspension in a compact heat exchanger. *Energies* 2019; 12: 1929.
49. Goodarzi M, Tlili I, Tian Z, et al. Efficiency assessment of using graphene nanoplatelets-silver/water nanofluids in microchannel heat sinks with different cross-sections for electronics cooling. *Int J Numer Methods Heat Fluid Flow* 2019; 30(1): 347–372.
50. Bahiraei M, Kiani Salmi H, and Safaei MR. Effect of employing a new biological nanofluid containing functionalized graphene nanoplatelets on thermal and hydraulic characteristics of a spiral heat exchanger. *Energy Convers Manag* 2019; 180: 72–82.